# Classical and Quantum Dynamics of 2D Optical Lattices

Presented by Eric Horsley
Department of Physics
The University of Texas at Austin

In partial fulfillment of the requirements for graduation with the Deans Scholars Honors Degree in Physics

| | |
|---|---|
| Prof. Linda Reichl<br>Supervisor | Date |
| Prof. Greg Sitz<br>Honors Adviser in Physics | Date |

**Abstract**

Here we present the work and results of studies on a two-dimensional optical lattice. The initial work on the classical dynamics describes the onset of chaos using action-angle variables and techniques developed by Walker and Ford [1]. Having documented the classical transition to chaos, using a technique called the discrete variable representation, we calculate the eigenvalues and eigenvectors of the two-dimensional optical lattice Hamiltonian operator. The surprising fidelity of these numerical results to the true values (which can be verified for a certain parameter value) will hopefully allow for the future study of level repulsion and the development of quantum phase space distributions (e.g. the Wigner and Husimi quasi-probability distributions).

# Acknowledgements

Research is a tale which never ends, and so it represents a considerable challenge to understand what the story has been up to now. In classes we are taught what is foundational in our field, and then slowly we get closer to the boundary of knowledge. This journey has at times, and I'm sure it always will, seemed daunting, but I have had wonderful mentors whose guidance has made the journey something to enjoy. I could never hope to thank every teacher and mentor I've had lest this section become a thesis unto itself, so I will restrict myself to those directly related to my education in physics and those memories which come immediately to mind.

My time with physics began in high school with Mr. Richard Gossman and Dr. Charles Reidl. This is an instance in life where the whole is greater than the sum of the parts. The synergy of the mathematics and physics they taught is something I hope to be able to achieve in my own teaching one day. Also, they showed me what it meant to not be lazy in my thinking. If I asked a questions and they knew I could find the answer on my own, then they would make me sort it out. There isn't much else which can liberate the mind to the extent that that lesson did. In addition to a strong foundation in math and physics, the general wisdom about life they proffered will be with me forever.

I thank Professor Sonia Paban for her persistence in trying to teach me even when my stubbornness seemed insurmountable. As an example of her

persistence, I thank her for not thinking too much less of me for botching integration by parts and insisting I was doing it correctly. Any quantum mechanics I know well is due to her, and the rest I simply didn't pay enough attention. During the time of graduate school applications she said something which I will never forget; intelligence can only take you so far, every scientist has to have ideas.

Next I thank Professor Linda Reichl. From her I learned classical dynamics, and I found the course so interesting that I asked to begin doing research related to chaos with her. She has been my adviser and mentor for nearly three years at the time of writing this thesis. Her excitement about physics reminded me of my own interest at times when I had forgotten. An important lesson she taught me was to always try to solve and understand the simple problem before tackling the more difficult one. Needless to say this lesson had to be repeated many times. Always insisting that classes come first, she was thinking of my future in physics even when I wasn't.

If there is any group of people you learn the most from it is your peers. There are too many wonderful memories to share here, so I hope it is clear from our conversations that I cherish and will continue to learn from them all.

How could I ever not thank my parents? I have always had their support in whatever I chose to do. Although, I know they are relieved that I chose to give up on studying music at university. I hope that whatever I may end up doing in life makes them proud. I have always found it hard to call any

place "home" when they and my brother weren't there. That I have always had such a home brings me peace whenever life may seem difficult.

# Contents

# List of Figures

# Chapter I

# Introduction

In physics we build models and theories with certain phenomena in mind which we hope to explain the dynamics of, and hopefully, having developed a theory from general enough principles, more phenomena than what was originally hoped for can be understood. The beginnings of "quantitative" physics with Newton and predecessors were obsessed with the celestial; the heavenly bodies were their playground. Even early civilizations, such as the Mayans, had developed sophisticated astronomical systems which could predict the coming of the solstice and equinox. Yet, the work of the Mayans was really only descriptive; it lacked explanatory power. But the work of Newton marks an enormous intellectual leap; Newton's laws are an explanatory tool. In all its might this new quantitative science, what is now called, classical physics was thought to apply to all length scales in the known Universe ("known" is a nice way, it seems to me, of describing our perpetual

naïveté). Alas, we look back now and realize, despite classical physics describing the world in a far broader way than it set out to, that such a hope was shortsighted. Nevertheless, it also led to us to broaden the way we think about the world and develop more elaborate, and sometimes intuition defying, theories. Even with these relatively modern theories, looking back on the rich history of physics, we begin to see the apparent discontinuity of our intellectual evolution. Quantum mechanics developed out of the study and explanation of atomic spectra; the world on the order of an Angstrom. So, considerations for quantum-classical correspondence are important not only for understanding mesoscopic scales but also for the philosophical coherence of the physicist. If quantum theory predicts very well the dynamics of a few atoms, and classical physics handles the dynamics of the rockets flying between the Earth and the ISS, then shouldn't quantum mechanics also be able to produce the dynamics of the rocket? If the physicist were to believe otherwise, then they would relegate an entire scale of physics outside the purview of our current body of knowledge. If you like, results of quantum mechanics can be seen in the large scale world [2]. For instance, without the Pauli exclusion principle how could we ever hope to understand the stability of rigid bodies; or even the evolution of stars? This leads us to the underlying purpose for the tools developed in this thesis. We know that there exists chaos in classical systems; what is the manifestation or the underlying dynamics of the quantum mechanics which lead to this? Where in the world is quantum chaos?

# Chapter II

# Background and Motivation

Many systems have been studied and many tools developed to investigate chaos in classical and quantum mechanics. In the classical world we use the tools developed by Poincaré to study the evolution of trajectories in a $2N$ dimensional phase space in a space of dimension less than $2N$ (here $N$ is the dimension of the configuration space; also called the degrees of freedom). This is accomplished by looking at the surface specified after choosing a value for one of the configuration space coordinates. We call this a surface of section (SoS). In an energy conserving system the trajectories will live on a $2N-1$ dimensional surface. This is a general result, and further integrals of the motion will act to reduce the dimension of the phase space. A 2 degree of freedom system which conserves energy and and an angular momentum-like quantity will lie on the surface of a 2-torus. A system whose number of integrals of motion is equal to its degrees of freedom is said to be integrable.

The existence of action-angle coordinates, which we use extensively here, depends intimately on the form of the level sets generated by integrals of motion (Liouville-Arnold theorem). In addition, there are systems which have integrals of the motion that number more than $N$, and such systems are called super-integrable. The Kepler problem is a well known example of such a system.

For the quantum mechanics, we employ a numerical approach known as the Discrete Variable Representation to get the eigenvalues and eigenvectors of the Hamiltonian. The approach is favored over the usual variational technique for reasons explained in the chapter on quantum mechanics. With these eigenvalues and eigenvectors it will be possible to look at the level spacing data and quasi-probability distributions (e.g. Wigner and Husimi distributions [3][4][5]) which help to identify chaos in the quantum system.

The classical quantum correspondence is a fairly large topic of which this thesis could never hope to convey a broad understanding. In fact, restricting ourselves to classical chaos and its manifestations in the quantum regime is still a remarkably sprawling beast. We are left to consider a single model chaotic Hamiltonian, but we do have the added benefit of working with a physically realizable Hamiltonian [6][7]. The last fifteen years have seen a great deal of research into optical lattices in both theory and experimental work [7][8][9][10][11]. The optical lattice is of particular interest because it allows for the study of classical-quantum correspondence as it relates to the manifestation of classical chaos in the quantum regime. Some of that work,

both theoretical and experimental, has looked at the influence of classical chaotic dynamics on quantum tunneling in a time-periodic potential [11][10]. The theoretical work found good agreement with the experimental work. The full scope of the classical dynamics of the Hamiltonian used by M. Greiner *et al.* [7] and Hemmermich *et al.* [6] has yet to be investigated and that is where we first direct our attention. Some of the results here appear in a paper published in Physical Review E by the author and collaborators [12]. The experimental set up is realized by having two pairs of counter-propagating lasers form standing waves. The Hamiltonian generated by these counter-propagating lasers is given below.

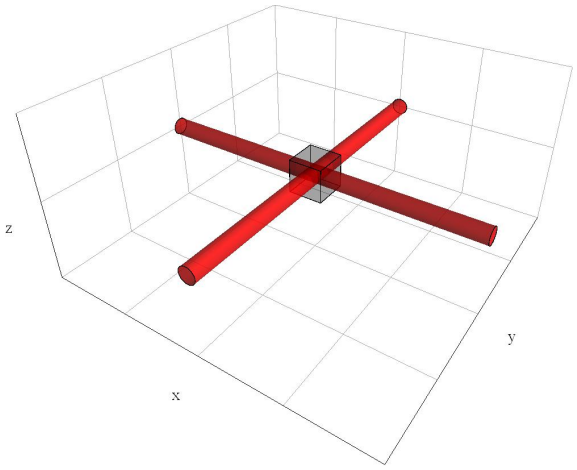


Figure II.1: A schematic of counter-propagating lasers. The grey box encloses the region in which atoms are loaded into the optical lattice.

$$H' = \frac{{p'_{x'}}^2}{2m} + \frac{{p'_{y'}}^2}{2m} + U_0(\cos^2 k_L x' + \cos^2 k_L y' + 2\cos\phi\cos\theta\cos k_L x'\cos k_L y') \tag{II.1}$$

Here $\theta$ defines the angle between the polarization vectors of the two pairs of counter-propagating lasers and $\phi$ the relative phase between the lasers. A plot of this setup is given at the top of the page. The Greiner experiment used Rubidium atoms and a laser wavelength of 852 nm. The dimensionless form of the Hamiltonian is achieved by the following change of variables: $p'_{x'} = \hbar k_L p_x,\ p'_{y'} = \hbar k_L p_y,\ x' = \frac{x}{k_L},\ y' = \frac{y}{k_L},\ H' = H\frac{\hbar^2 k_L^2}{2m}, U_0 = U\frac{\hbar^2 k_L^2}{2m}$. The resulting Hamiltonian is

$$H = p_x^2 + p_y^2 + U(\cos^2(x) + \cos^2(y) + 2\alpha\cos(x)\cos(y)). \tag{II.2}$$

Note that the coefficient of the nonseparable term has been combined such that $\alpha = \cos\phi\cos\theta$.

The Hamiltonian for the optical lattice can be arrived at both classically [13] and quantum mechanically [14]. Under the assumptions given in [14] the quantum mechanical result can be seen to come from a dipole interaction in a two-level system.

The starting Hamiltonian for this dipole interaction of a two-level system can be written in the following way.

$$\hat{H}_{atom} = \mathbb{1} \otimes (E_g \left|g\right\rangle\!\left\langle g\right| + E_e \left|e\right\rangle\!\left\langle e\right|) + (\tfrac{\hat{p}_x^2}{2m} + \tfrac{\hat{p}_y^2}{2m}) \otimes (\left|g\right\rangle\!\left\langle g\right| + \left|e\right\rangle\!\left\langle e\right|) \quad \text{(II.3)}$$

$$\hat{H}_{int} = -\vec{d} \cdot \vec{E}(x, y, t) \quad \text{(II.4)}$$

For simplicity we subtract a constant energy $E_g$ from the two-level system Hamiltonian such that the ground state will now have an eigenvalue of zero. Defining $E_e - E_g \equiv \hbar\omega_{at}$ the Hamiltonian becomes:

$$\hat{H}_{atom} = \mathbb{1} \otimes \hbar\omega_{at} \left|e\right\rangle\!\left\langle e\right| + (\frac{\hat{p}_x^2}{2m} + \frac{\hat{p}_y^2}{2m}) \otimes (\left|g\right\rangle\!\left\langle g\right| + \left|e\right\rangle\!\left\langle e\right|) \quad \text{(II.5)}$$

This sets the Hamiltonian into an analogous form as the one translational degree of freedom Hamiltonian used in the appendix of [14]. The derivation for our two translational degree of freedom Hamiltonian follows in similar fashion.

# Chapter III

# Classical Chaos

## 1 Early work

All the work in the remainder of this thesis deals exclusively with the dimensionless Hamiltonian motivated earlier and given again here.

$$H = p_x^2 + p_y^2 + U(\cos^2(x) + \cos^2(y) + 2\alpha\cos(x)\cos(y)). \tag{III.1}$$

Hamilton's equations are computed in the usual way

$$\dot{p_x} = 2U\left(\cos(x)\sin(x) + \alpha\sin(x)\cos(y)\right)$$

$$\dot{x} = 2p_x$$

$$\dot{p_y} = 2U\left(\cos(y)\sin(y) + \alpha\cos(x)\sin(y)\right)$$

$$\dot{y} = 2p_y$$

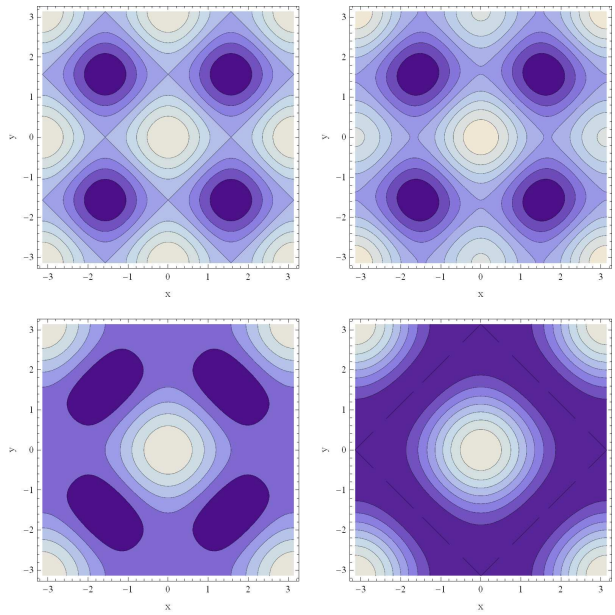

Figure III.1: Counter plots for $\alpha = 0$ (top left), $\alpha = 0.1$ (top right), $\alpha = 0.5$ (bottom left), and $\alpha = 1.0$ (bottom right)

Chaos appears in the phase space for $\alpha \neq 0$, and if $\alpha = 0$ then the system becomes integrable by virtue of the recovery of an integral of motion. The integrable system is analogous to a two-dimensional pendulum. Contour plots are given for what we have found are values of $\alpha$ which show most of the characteristic dynamics.

The scheme for producing a surface of section is relatively simple for systems with one or two degrees of freedom. In higher dimensions one needs to study additional structures in the phase space which allow you to visualize the dynamics of the system, because, in general, a sufficient number of integrals of the motion will not exist to the lower the dimensionality of the

space on which the trajectories live (normally hyperbolic invariant manifolds or NHIMs are an example of such a structure; see [15])

We develop our surfaces of section as follows (a general approach):

1. Chose a restriction of phase space to a specific value of one of the degrees of freedom ($y = \frac{\pi}{2}$ in our case).

2. Chose an appropriate set of initial conditions for $(x, p_x)$, and then, by energy conservation, this will fix what $p_y$ must be.

3. These initial conditions can now be used to numerically solve (or analytically in the $\alpha = 0$ case) Hamilton's equations.

4. With all of the phase space variables now known as a function of time, one must identify all those times for which $y(t_i) = \frac{\pi}{2}$. Furthermore, times should only be included which correspond to a crossing of the plane with $p_y(t_i) > 0$ (this is by convention).

5. Now the position and momentum in the x-direction may be evaluated at the appropriate $t_i$ values, $(x(t_i), p_x(t_i))$. These points, when plotted, give you the surface of section.

In figures III.2a, III.2b, and III.2c we attempt to show the breadth of structure in the phase space across couplings and energies below the max height of the potential.

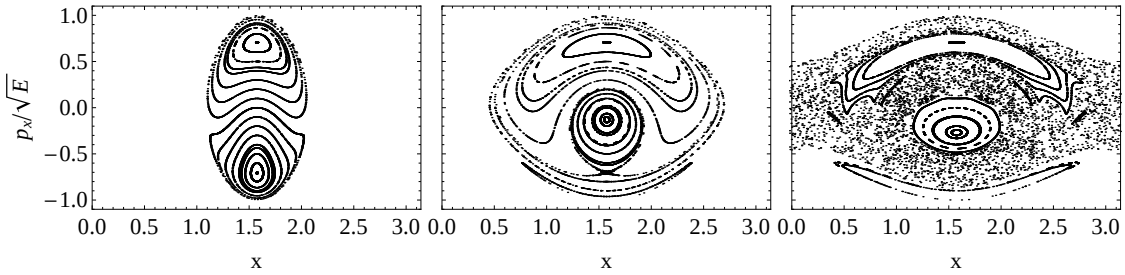


(a) Plots where $\alpha = 0.1$, and for which $V_{max} = 44$. The energies for each plot from left to right are the following: $E = \frac{1}{10}V_{max} = 4.4$, $E = \frac{3}{8}V_{max} = 16.5$, $E = \frac{5}{8}V_{max} = 27.5$

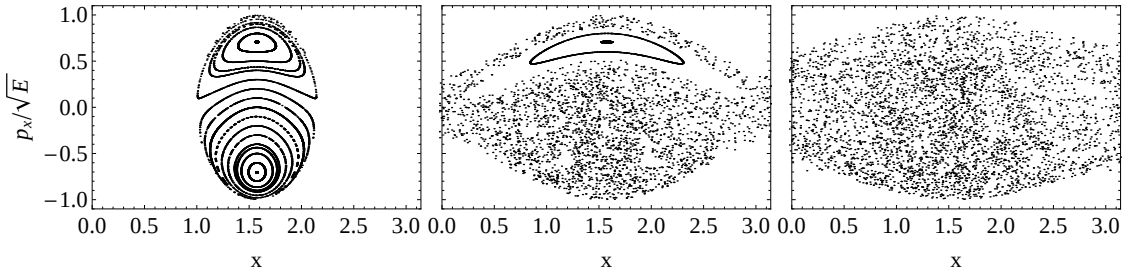


(b) Plots where $\alpha = 0.5$, and for which $V_{max} = 60$. The energies for each plot from left to right are the following: $E = \frac{1}{10}V_{max} = 6$, $E = \frac{3}{8}V_{max} = 22.5$, $E = \frac{5}{8}V_{max} = 37.5$

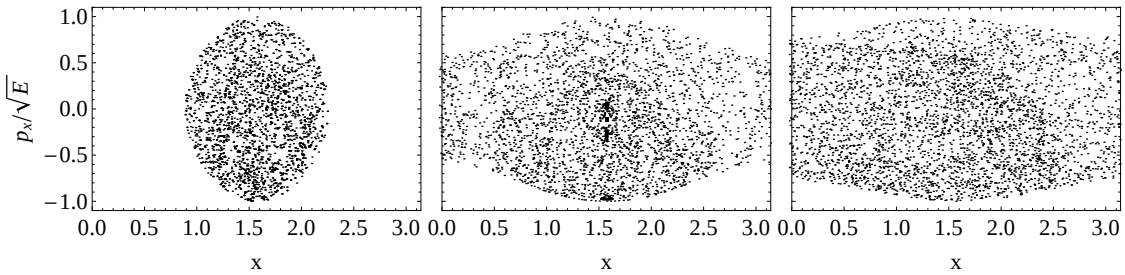


(c) Plots where $\alpha = 1.0$, and for which $V_{max} = 80$. The energies for each plot from left to right are the following: $E = \frac{1}{10}V_{max} = 8$, $E = \frac{3}{8}V_{max} = 30$, $E = \frac{5}{8}V_{max} = 50$

Figure III.2: Overview of phase space structure for $E < V_{max}$ and various couplings.

## 2 Walker-Ford Libration

Ignoring the coupling term, the dimensionless Hamiltonian, up to a coordinate transformation, reduces to a two dimensional uncoupled pendulum: $H_x = p_x^2 + U\cos^2(x)$ and $H_y = p_y^2 + U\cos^2(y)$. The pendulum system lends itself to a convenient transformation to action-angle variables. This coordinate transformation, $(x, y, p_x, p_y) \to (\theta_x, \theta_y, J_x, J_y)$, is accomplished through the following transformation equations:

$$\begin{aligned} p_x &= k_x\sqrt{U}\,\mathrm{cn}\left[\tfrac{2\mathbb{K}(k_x{}^2)\theta_x}{\pi}, k_x{}^2\right] \quad x = \tfrac{\pi}{2} + \sin^{-1}\left[k_x\,\mathrm{sn}\left[\tfrac{2\mathbb{K}(k_x{}^2)\theta_x}{\pi}, k_x{}^2\right]\right] \\ p_y &= k_y\sqrt{U}\,\mathrm{cn}\left[\tfrac{2\mathbb{K}(k_y{}^2)\theta_y}{\pi}, k_y{}^2\right] \quad y = \tfrac{\pi}{2} + \sin^{-1}\left[k_y\,\mathrm{sn}\left[\tfrac{2\mathbb{K}(k_y{}^2)\theta_y}{\pi}, k_y{}^2\right]\right] \end{aligned} \tag{III.2}$$

These transformation are only defined for $E_x, E_y < U$ (the libration regime). They can be obtained by quadrature. For a fixed energy $E_x$ the momentum takes the form:

$$p_x = \sqrt{E - U\cos^2(x)} \tag{III.3}$$

Now using Hamilton's equation for $\dot{x}$ we get the following:

$$\dot{x} = 2p_x = 2\sqrt{E_x - U\cos^2(x)} \tag{III.4}$$

Now the quadrature can be written down

$$2\int_{t_0}^{t'} dt = \int_{x'(t_0)}^{x'(t')} \frac{dx}{\sqrt{E_x - U\cos^2(x)}} \tag{III.5}$$

This integral can be evaluated analytically [16](although, not in terms of finitely many elementary functions), and then inverted to solve for $x(t)$. The angular variable in the action-angle coordinates is linear in time allowing for a simple substitution to find $x(\theta_x)$.

Furthermore, the action is given by the following expression

$$J_x = \frac{1}{2\pi}\oint dx\ p_x = \frac{2}{\pi}\sqrt{U}\left[\mathbb{E}(\kappa_x) - (1-{\kappa_x}^2)\mathbb{K}(\kappa_x)\right] \tag{III.6}$$

where the modulus ${\kappa_x}^2 = E_x/U$ and $\mathbb{K}(\kappa)$ and $\mathbb{E}(\kappa)$ are complete elliptic integrals of the first and second kind, respectively. where $\mathrm{sn}\,(h_x, \kappa_x)$ and $\mathrm{cn}\,(h_x, \kappa_x)$ are the Jacobi "sn" and "cn" functions as defined in [16], respectively, and $h_x = \frac{2}{\pi}\mathbb{K}(\kappa_x)\theta_x$ The Jacobian of this transformation is equal to one, and therefore canonical. Exchange $x \to y$ and you have the correct expressions for $H_y$.

In terms of the action-angle variables, the full Hamiltonian takes the form

$$\begin{aligned} H &= E_x + E_y + 2U\kappa_x\kappa_y\ \alpha\ \mathrm{sn}\,(h_x,\kappa_x)\,\mathrm{sn}\,(h_y,\kappa_y) \\ &= E_x + E_y + \alpha U\frac{\pi^2}{\mathbb{K}(\kappa_x)\mathbb{K}(\kappa_y)}\sum_{n_x=0}^{\infty}\sum_{n_y=0}^{\infty} f_{n_x}(\kappa_x)f_{n_y}(\kappa_y) \\ &\quad\times[\cos[(2n_x+1)\theta_x \pm 1(2n_y+1)\theta_y] \end{aligned} \tag{III.7}$$

where $f_{n_x}(\kappa_x) = \text{csch}\left[(2n_x+1)\frac{\pi}{2}\frac{\mathsf{K}'(\kappa_x)}{\mathsf{K}(\kappa_x)}\right]$, $\mathbb{K}'(\kappa_x) = \mathbb{K}(\sqrt{1-{\kappa_x}^2})$, and again take $x \to y$ and you have the equivalent definitions for the other degree of freedom. The Fourier series expansion of the Hamiltonian is obtained by expanding Jacobi "sn" functions in a Fourier series [16]. Eq. (III.7) gives us an expansion of the optical lattice Hamiltonian in terms of a sum of resonances in the libration regime. These resonances build up at the separatrices of the pendulum and this effect tracks the development of chaos. We find that the resonance with $(n_x, n_y) = (0, 0)$ lies farthest from the separatrices expected from the potential and is by far the largest resonance. The next few resonances, when isolated, appear to show near trivial structure (lines of near-constant action).

We can now follow an analysis first described by Walker and Ford [1]. We look at the Hamiltonian with $(n_x, n_y) = (0, 0)$ and the difference of cosines:

$$H^{-}_{L;0,0} = E_x + E_y + U\ \alpha\ \frac{\pi^2}{\mathbb{K}(\kappa_x)\mathbb{K}(\kappa_y)}\ f_0(\kappa_x) f_0(\kappa_y)\ \cos[\theta_x - \theta_y] = E \quad \text{(III.8)}$$

We will analyze the SoS of $(x, p_x)$ plotted every time $y = \frac{\pi}{2}$, and we will focus on the interval $0 \leq x \leq \pi$. This single term will give the entire phase space structure under the full optical lattice Hamiltonian at low energy and coupling. Note that the Hamiltonian when only one value is chosen for both $n_x$ and $n_y$ is integrable by virtue of an additional conserved quantity we call $\Gamma$. This can be seen immediately from Hamilton's equations in action-angle variables.

$$\Gamma^{\pm} = (2n_y + 1)J_x \mp (2n_x + 1)J_y \tag{III.9}$$

Where the $\pm$ choice is determined the the choice one makes for the Hamiltonians. Using $\Gamma$ to eliminate $J_x$ or $J_y$ we can build a surface of section by finding the values of the angles for which the energy is conserved. This method is somewhat difficult to implement depending on how well the function which you wish to know the roots of are behaved, so solving Hamilton's equations numerically in action-angle variables is preferred.

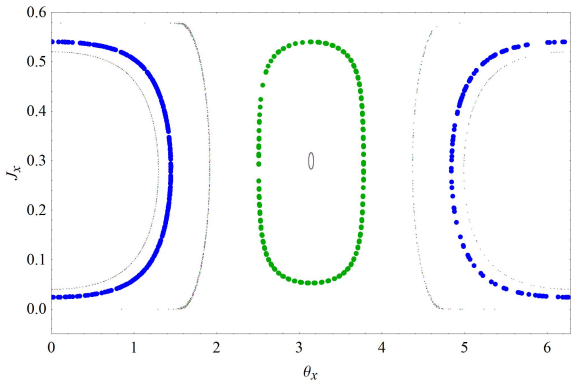


Figure III.3: A surface of section in the action angle coordinates for the Walker-Ford Hamiltonian with the topologically distinct types of trajectories colored blue and green. This is for $\theta = 0$ and $E = 5$

In the figures which follow, we plot a SoS of $(J_x, \theta_x)$ each time $\theta_y = 0$ for $\alpha = 0.1$. Figure III.3 corresponds to energy $E = 5$ and figure III.4 corresponds to energy $E = 5$ but transformed from the action-angle variables into Cartesian coordinates. For energies below about $E \approx 7.2$, the phase space shows no signs of chaos or internal separatrices, even though the coupling

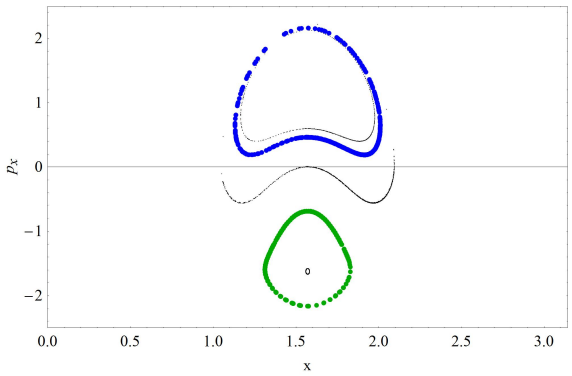


Figure III.4: The surface of section given by using the canonical transformation equations from action-angle to Cartesian coordinates.

between the degrees of freedom changes the topology of the lattice. The approximate separation of positive and negative $p_x$ in the SoS results from an asymmetry by the choice of $y = \frac{\pi}{2}$ with nonzero coupling. For $E > 7.2$ the resonance described above appears in the phase space. This bifurcation of the phase space will be a source of chaos different from the separatrix associated with the saddle points of the potential. In figure III.5 we show how the correspondence between the bifurcation appearing in the $(n_x, n_y) = (0, 0)$ and the full Cartesian system.

As $\alpha$ increases, the energy at which the resonance appears in the phase space increases and the energy of the saddle point decreases. At the same time the regions of chaos associated with these two sources grows and begin to merge.

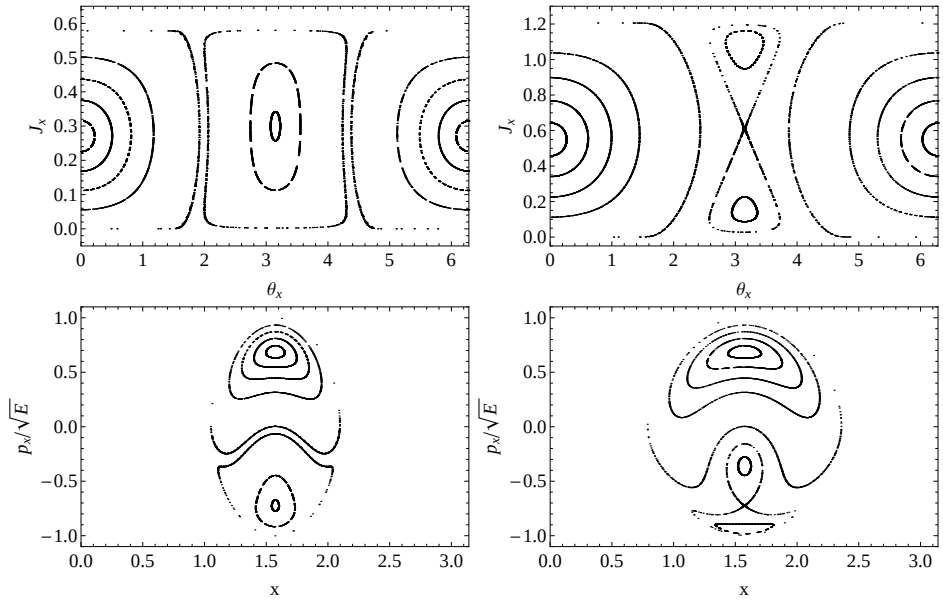


Figure III.5: In the first column, for energy $E = 5$, we show the action-angle SoS (top) and its transformation to Cartesian coordinates (bottom). The second column shows the same pairing but for $E = 10$; i.e. after bifurcation.

# 3 Walker-Ford Rotation

We begin again with the Hamiltonian (1) and transform to the action-angle coordinates, $(x, y, p_x, p_y) \rightarrow (\theta_x, \theta_y, J_x, J_y)$, defined in the rotation regime $(E > U)$. This is accomplished via the following transformation equations analogous to (2):

$$\begin{aligned} p_x &= \frac{\sqrt{U}}{\kappa_x}\,\mathrm{dn}\left[\frac{2\mathbb{K}(\kappa_x{}^2)\theta_x}{\pi}, \kappa_x{}^2\right] \quad x = \frac{\pi}{2} + \sin^{-1}\left[\kappa_x\,\mathrm{sn}\left[\frac{2\mathbb{K}(\kappa_x{}^2)\theta_x}{\pi}, \kappa_x{}^2\right]\right] \\ p_y &= \frac{\sqrt{U}}{\kappa_y}\,\mathrm{dn}\left[\frac{2\mathbb{K}(\kappa_y{}^2)\theta_y}{\pi}, \kappa_y{}^2\right] \quad y = \frac{\pi}{2} + \sin^{-1}\left[\kappa_y\,\mathrm{sn}\left[\frac{2\mathbb{K}(\kappa_y{}^2)\theta_y}{\pi}, \kappa_y{}^2\right]\right] \end{aligned} \tag{III.10}$$

These transformation are only defined for $E_x, E_y > U$ (the rotation

regime). These transformation equations, for small $\alpha$, are a good transformation for the full Hamiltonian (recall the fidelity of the lowest order resonance in the libration regime to the full Hamiltonian). Substituting (5) into (1) we get the Hamiltonian

$$H = E_x + E_y + 2U\cos\alpha\,\mathrm{sn}\left[\frac{2\mathbb{K}({\kappa_x}^2)\theta_x}{\pi}, {\kappa_x}^2\right]\mathrm{sn}\left[\frac{2\mathbb{K}({\kappa_y}^2)\theta_y}{\pi}, {\kappa_y}^2\right]. \quad \text{(III.11)}$$

Furthermore, the Jacobi sn functions can be expanded in a Fourier series and the Hamiltonian separated into the "minus" and "plus" parts

$$H^{\mp} = E_x + E_y \pm \frac{\pi^2\cos\alpha\sqrt{E_xE_y}}{\mathbb{K}({\kappa_x}^2)\mathbb{K}({\kappa_y}^2)}\sum_{n_x}\sum_{n_y} f_{n_x,n_y}\cos\left((2n_x+1)\theta_x \mp (2n_y+1)\theta_y\right) \quad \text{(III.12)}$$

$$f_{n_x,n_y} = \mathrm{csch}\left[(2n_x+1)\frac{\pi}{2}\frac{\mathbb{K}'({\kappa_x}^2)}{\mathbb{K}({\kappa_x}^2)}\right]\mathrm{csch}\left[(2n_y+1)\frac{\pi}{2}\frac{\mathbb{K}'({\kappa_y}^2)}{\mathbb{K}({\kappa_y}^2)}\right]$$

In a similar way to libration there exists another integral of the motion $\Gamma$. The same procedure from libration is used in this case. It's also difficult to work in rotation given that having more than one term of the series allows for energy exchange between $x$ and $y$ motions. It is then possible that $E_x < U$ or $E_y < U$ in which case the transformation equations for rotation are invalid. Certain initial conditions can still be studied in a many-term case if they are far enough from area of the phase space containing chaotic trajectories.

In figure III.6 we show various isolated resonances, and the commen-

tary which follows is with respect to those plots. Again, as in the libration regime, the lowest order term has largest nontrivial dynamical structure for sufficiently large energy. We make note that this structure has to be compared to the full structure at large energies because the chaotic sea consumes most of the available phase space near $E = 20$, or said another way, $\kappa_x, \kappa_y \to 1$. This implies that contribution from higher orders terms can not be neglected. The remaining three plots, though the $(n_x, n_y) = (1, 1)$ has some none trivial structure shown as a period-2 orbit, have relatively little structure of interest. Keeping in mind that the Hamiltonian for any isolated resonance is an integrable system we can not expect such simplistic behavior from a Hamiltonian with multiple resonances. Figure III.7 shows how when multiple resonances are included (all 4 from the previous figure) higher period orbits are generated near the separatrix and the overlap of such orbits leads to the development of the chaotic sea seen in the figure. See Appendix A for the code which generates these plots.

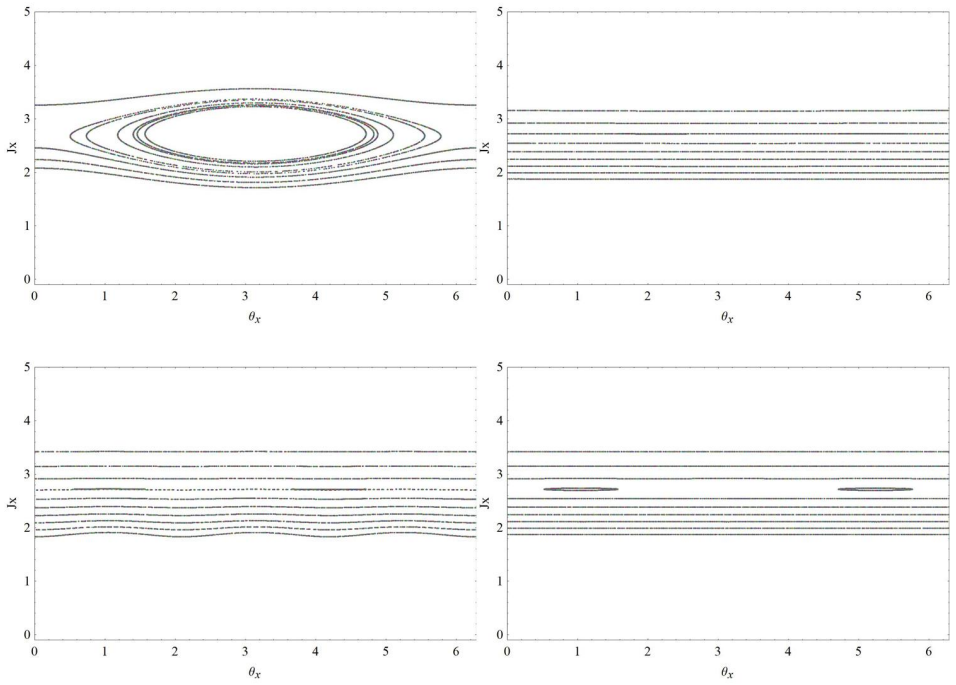


Figure III.6: Starting from the top left and reading left to right the SoS for a particular choice of resonance are: $(n_x, n_y) = (0, 0)$, $(n_x, n_y) = (0, 1)$, $(n_x, n_y) = (1, 0)$, and $(n_x, n_y) = (1, 1)$. The energy for all plots in dimensionless units is 80. Points are generated when the trajectory intersects $\theta_y = 2\pi$.

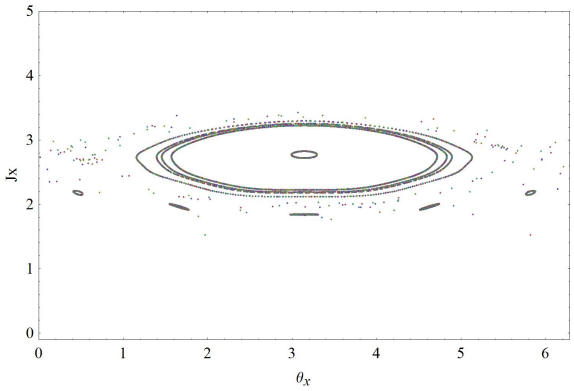


Figure III.7: A plot of the SoS generated from the Hamiltonian containing all four resonances: $(n_x, n_y) = (0, 0)$, $(n_x, n_y) = (0, 1)$, $(n_x, n_y) = (1, 0)$, and $(n_x, n_y) = (1, 1)$. The energy for all plots in dimensionless units is 80. Points are generated when the trajectory intersects $\theta_y = 2\pi$.

# Chapter IV

# Quantum States and the DVR

## 1 The Discrete Variable Representation

The numerical technique that inspires our approach here is called the discrete variable representation (DVR) [17][18]. We prefer the DVR technique over the usual variational method where the matrix elements of the potential are found in the following way:

$$V_{ij} = \int_a^b \psi_i^*(x)\, V(x)\, \psi_j(x) \mathrm{d}x \tag{IV.1}$$

where the set of $\{\psi_i\}$ make up an orthonormal basis for the Hilbert space. In most cases the orthonormal basis functions are not eigenvectors of the potential energy operator, so in the worst case for a truncated basis of $N$ functions there are $N^2$ integrals to compute. To illustrate the convenience

of the DVR imagine that we were to take as our basis the eigenstates of the position operator (PO). That is, those states for which $\hat{Q}\,|x\rangle = x\,|x\rangle$. A "matrix element" (since the spectrum of the position operator is continuous the use of the word matrix here is heuristic) of the potential energy operator would look like:

$$\begin{aligned} V(\hat{Q}) &= \int V(\hat{Q})\,|x\rangle\,\langle x|\,\mathrm{d}x \\ &= \int V(x)\,|x\rangle\,\langle x|\,\mathrm{d}x \end{aligned}$$

Now act with $V(\hat{Q})$ on some general position eigenstate $|x'\rangle$.

$$\begin{aligned} V(\hat{Q})\,|x'\rangle &= \int V(\hat{Q})\,|x\rangle\,\langle x|x'\rangle\,\mathrm{d}x \\ &= \int V(x)\,|x\rangle\,\delta(x-x')\mathrm{d}x \\ &= V(x')\,|x'\rangle \end{aligned}$$

Thus you can see that in this basis the operator is diagonal. Now, just as one must truncate the basis of functions in the variational method to do computations, we do the same for the position eigenstates which we just established were eigenstates of the potential energy operator. What we then have is a uniformly spaced grid over an interval which is given by the periodicity of the lattice. The set of all grid points $\{x_i\}$ then have the following

property with the potential energy:

$$V_{ij} = V(x_i)\delta_{ij} \tag{IV.2}$$

Furthermore, we can generate this grid with the basis functions $\psi_i$ from earlier by finding the eigenvalues of the position operator in the truncated basis (POTB). The corresponding eigenvectors become Dirac delta functions in the limit of the number of basis functions going to infinity.

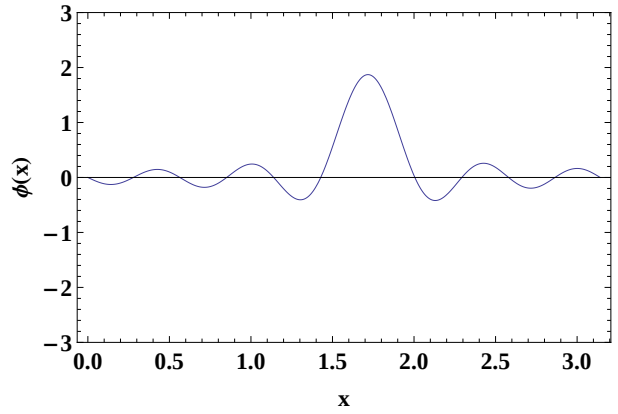


Figure IV.1: A plot of the eigenvector of the POTB for a basis consisting of only 10 sine functions. One can read off the eigenvalue associated with such an eigenvector; in this case $x_{eig} = 1.71664$.

A plot of the POTB eigenvectors is shown above for both the one- and two-dimensional case in Figures IV.1 and IV.2. Had we kept with the variational approach we would be forced to evaluate the potential energy elements with an integral over the POTB eigenfunctions; thus no computing time is saved. This is, if you like, a moral and economical justification for evaluating

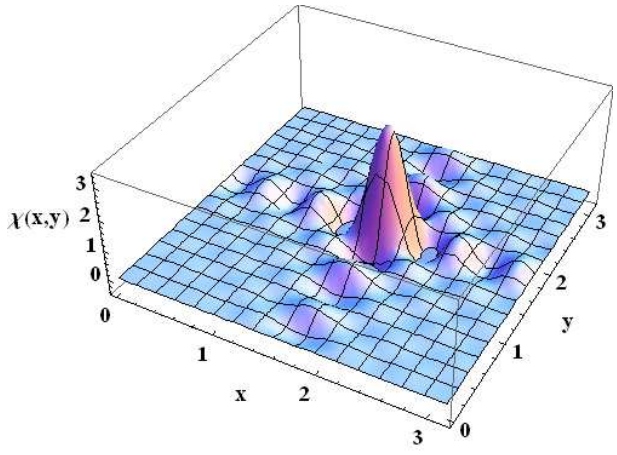


Figure IV.2: A plot of the product of eigenvectors of POTB for both the $x$ and $y$ degrees of freedom. A basis of 10 sine functions is used for each dimension. One can read off the eigenvalue associated with such an eigenvector; in this case $x_{eig} = 3.43327, y_{eig} = 3.43327$.

the potential energy at the grid points, respectively. Furthermore, the form of the kinetic energy given the basis states is ([17]):

$$T_{ii'} = -\frac{\hbar^2}{2m}\Delta x \sum_{n=1}^{N-1} \psi_n(x_i)\psi_n''(x_{i'}) \tag{IV.3}$$

where $\Delta x$ gives the spacing between grid points, and, like before, $\{x_i\}$ are the grid points and $\psi_n''$ is the second derivative of the basis function $\psi_n$. It is fortunate that we have a periodic potential for which trigonometric functions are a natural choice of basis. Both the sine and cosine are eigenfunctions of the Laplacian operator. It is an interesting question to ask whether this helps to tame errors in the method, or if a consistent approach should be taken in evaluating each piece of the Hamiltonian (we have effectively treated the

kinetic energy with the continuum as opposed to the grid); further investigation is needed. The variational approach has one advantage that is lost with the DVR; numerical results for the energy eigenvalues are not guaranteed to be bounded below by the true eigenvalue. By approximating the full integrals that would normally be used to compute the potential energy matrix we are no longer solving a variational problem.

# 2 1D & 2D Quantum Pendulum

Let's first consider the no coupling, one dimensional version of our Hamiltonian. This Hamiltonian is essentially a one-dimensional pendulum for which periodic Mathieu functions are the known the solutions.

$$\hat{H}_{1D} = \hat{p}_x^2 + U\cos^2(\hat{x}) \tag{IV.4}$$

The Mathieu differential equation was first published in 1868 ([19]). By writing down the time-independent Schrödinger equation in the position basis, and using the appropriate dimensionless momentum operator, the Mathieu differential equation can be recovered as follows:

$$\begin{aligned}
\hat{p}_x \to -i\frac{d}{dx}, \quad \hat{x} \to x \\
\hat{H}_{1D}\psi = \left(-\frac{d^2}{dx^2} + U\cos^2(x)\right)\psi = E\psi \\
\frac{d^2\psi}{dx^2} + \left[(E - \frac{1}{2}U) - 2(\frac{1}{4}U)\cos(2x)\right]\psi = 0
\end{aligned}$$

The use of parentheses inside the square brackets is to show the equivalence between the form of Mathieu's equation built into *Mathematica* and the result given above. That equation is:

$$\frac{d^2y}{dx^2} + [a - 2q\cos(2x)]\, y = 0 \tag{IV.5}$$

Using the characteristic values for even and odd Mathieu functions, which are functions of the quantum number for the energy level and the value of $q$, the eigenvalues can be computed immediately. Here $q = \frac{U}{4}$, and remembering that $U$ is a just a parameter of our Hamiltonian, q is known. The $a$ in this equation is Mathieu's charcterictic value for even/odd Mathieu functions (What basis we use decides if it is even or odd). We chose which quantum number we wish to know the associated energy for, and then substituting these into:

$$E = a + \frac{U}{2} \tag{IV.6}$$

we have the energy eigenvalues.

# 3 Optical Lattice Eigenstates and Eigenvalues

It makes life simpler to consider the Hamiltonian in the following way:

$$\hat{H} = \hat{p}_x^2 \otimes \hat{\mathbb{1}} + \hat{\mathbb{1}} \otimes \hat{p}_y^2 + U\left(\cos^2\hat{x} \otimes \hat{\mathbb{1}} + \hat{\mathbb{1}} \otimes \cos^2\hat{y} + 2\alpha\cos\hat{x} \otimes \cos\hat{y}\right) \tag{IV.7}$$

The benefit to viewing at the Hamiltonian in this way, which may seem obscure at first look, is that we can easily compute each term in whatever basis is computationally the easiest. After doing so we can transform to a common basis for all terms. At the very end we will find the eigenvalues and eigenvectors of the Hamiltonian in the following bases:

$$\mathcal{B}_x = \{\sin(nx) : n = 1, \ldots, N\}$$
$$\mathcal{B}_y = \{\sin(ny) : n = 1, \ldots, N\}$$

The following describes how to go through the actual computation of the energy eigenstates from start to finish (this models how the code was written in *Mathematica*; see Appendix B for actual code).

Our first goal is generate the grid. To do this we need a truncated set of orthonormal basis functions. Normalizing over the interval $[0, \pi]$ these basis functions are

$$\psi_m(x) = \sqrt{\frac{2}{\pi}} \sin(mx)$$
$$\phi_n(y) = \sqrt{\frac{2}{\pi}} \sin(ny)$$

Now we compute the POTB in this normalized basis. You will note that the results for $\hat{x}$ and $\hat{y}$ will be the same so there is no reason to compute the following matrix twice.

$$\hat{x}_{ij} = \int_0^\pi \psi_i^*(x)\, x\, \psi_j(x) \mathrm{d}x$$

The eigenvalues of this matrix constitute the grid. For a basis truncated after 10 functions the eigenvalues for the following:

```
{0.257164, 0.549337, 0.84139, 1.13324, 1.42496, 1.71664, 2.00836,
2.3002, 2.59226, 2.88443}
```

Furthermore, the eigenvectors of this matrix will be used to construct a linear transformation between the sine basis and the discrete position basis. I will denote this matrix of eigenvectors by $\mathbf{P}$. So, the $i$-th column of $\mathbf{P}$ will be the eigenvector corresponding to the the $i$-th grid point ($x_i$). In the code, found in Appendix B below, $\mathbf{P}$ is equivalent to the transpose of what is called "NumEigX2". This matrix is the same for both degrees of freedom. To reiterate, we move to this discrete position basis such that the potential energy will be diagonal. Remember, these eigenvectors in the limit of the number of basis functions going to infinity would become Dirac delta functions. Earlier we showed what one of these eigenstates of position looks like in the truncated basis; an approximation to the Dirac delta function.

We now need to compute both the kinetic energy and potential energy. The kinetic energy is computed most easily in the sine basis since the sine function is an eigenfunction of the second derivative. Therefore we can just write the eigenvalues down the diagonal. Note that the subscripts on the matrices which follow all refer to which degree of freedom is being dealt with.

$$\mathbf{K}^x_{ij} = i^2 \delta_{ij}$$

With an identical expression for kinetic energy coming from the other degree of freedom (bolding is used to denote evaluation in the sine basis). The potential energy is computed as follows:

$$U^x_{ij} = \cos^2(x_i)\delta_{ij}$$

where $x_i$ should be thought of as the i-th entry of the vector of eigenvalues. As before, an identical expression is written for the other degree of freedom. For the coupling term we will need the following as well

$$V^x_{ij} = \cos(x_i)\delta_{ij}$$

Before we can construct the Hamiltonian we must return every matrix to the same basis. We chose to leave the kinetic energy as is; in the sine basis. We transform all the potential energy matrices into the sine base using the matrix of eigenvectors ,$\mathbf{P}$, described earlier. Bold letters will be used to denote matrices in the sine basis.

$$\mathbf{U}^x = \mathbf{P}\, U^x\, \mathbf{P}^{-1}$$

$$\mathbf{U}^y = \mathbf{P}\, U^y\, \mathbf{P}^{-1}$$

$$\mathbf{V}^x = \mathbf{P}\, V^x\, \mathbf{P}^{-1}$$

$$\mathbf{V}^y = \mathbf{P}\, V^y\, \mathbf{P}^{-1}$$

This may all seem very compartmentalized, but the choice is to deal with

10x10 matrices for each degree of freedom or 100x100 matrices utilizing a basis which incorporates both degrees of freedom in defining the basis. In following the former technique we can utilize some useful properties of the Kronecker product [20]. In particular, if matrices $\mathbf{A}$ and $\mathbf{B}$ both have a set of linearly independent eigenvectors, then the Kronecker product of an eigenvector of $\mathbf{A}$ and $\mathbf{B}$, respectively, is an eigenvector of the Kronecker product of $\mathbf{A}$ and $\mathbf{B}$. Secondly, given that we deal here with diagonalizable matrices let $\mathbf{P}_A$ and $\mathbf{P}_B$ be the matrices of eigenvectors for $\mathbf{A}$ and $\mathbf{B}$, respectively. We can now initiate a basis change in the following way:

$$(\mathbf{P}_A \otimes \mathbf{P}_B)^{-1}(\mathbf{A} \otimes \mathbf{B})\,(\mathbf{P}_A \otimes \mathbf{P}_B) = (\mathbf{P}_A^{-1}\,\mathbf{A}\,\mathbf{P}_A) \otimes (\mathbf{P}_B^{-1}\,\mathbf{B}\,\mathbf{P}_B)$$

Rewriting the Hamiltonian defined at the beginning of this section with the notation developed in the ensuing discussion

$$\hat{H} = \mathbf{K}^x \otimes \hat{\mathbb{1}} + \hat{\mathbb{1}} \otimes \mathbf{K}^y + U\left(\mathbf{U}^x \otimes \hat{\mathbb{1}} + \hat{\mathbb{1}} \otimes \mathbf{U}^y + 2\alpha \mathbf{V}^x \otimes \mathbf{V}^y\right)$$

The circled cross is the tensor product which for matrices is the Kronecker product. These Kronecker products are easily carried out in *Mathematica*, and just as quickly we can get the eigenvectors and eigenvalues of the Hamiltonian. The actual *Mathematica* file can be found in Appendix B. This is not the entire story. This procedure has to be replicated for a basis of cosines in each degree of freedom, and twice for one degree of freedom in the sine basis and one in the cosine basis. However, little additional computation is needed

once one does all the work in the sine-sine basis and cosine-cosine basis; these results have all the necessary components for the sine-cosine/cosine-sine basis computation. The accuracy of this scheme can be verified since, in the integrable case ($\alpha = 0$), the solution to the time-independent separable Schrodinger equation is known. These are the periodic Mathieu functions mentioned already. We can compute in *Mathematica* the characteristic value, called $a$ previously, and compute the energy eigenvalue for each degree of freedom. In the table below we compare the DVR technique with these "exact" values, and we take as a basis 10 sine functions in both degrees of freedom.

| DVR | Exact |
|---|---|
| 8.41984 | 8.41984 |
| 16.30943 | 16.30938 |
| 16.30943 | 16.30938 |
| 23.44655 | 23.44625 |
| 23.44655 | 23.44625 |
| 24.19901 | 24.19892 |
| 30.85927 | 30.85814 |
| 30.85927 | 30.85814 |
| 31.33613 | 31.33579 |
| 31.33613 | 31.33579 |

Including only 10 basis functions in each degree of freedom our percent error is on the order of 0.01% for the 10 lowest lying energy eigenstates. However, the error does grow as one looks at the larger eigenvalues. In gen-

eral, one would always want to work with on the order of 100 basis functions, which given the methods accuracy for 10 basis functions, will probably provide the necessary accuracy for any further applications. That would include the level spacing distribution and the development of quasi-probability distributions (i.e. Wigner and Husimi distributions). The plots below show the evolution of the ground state as the coupling is increased from 0 to 1. With the large central peak developing at $(0, 0)$ in the potential the wave functions become confined to the lanes surrounding the maximum.

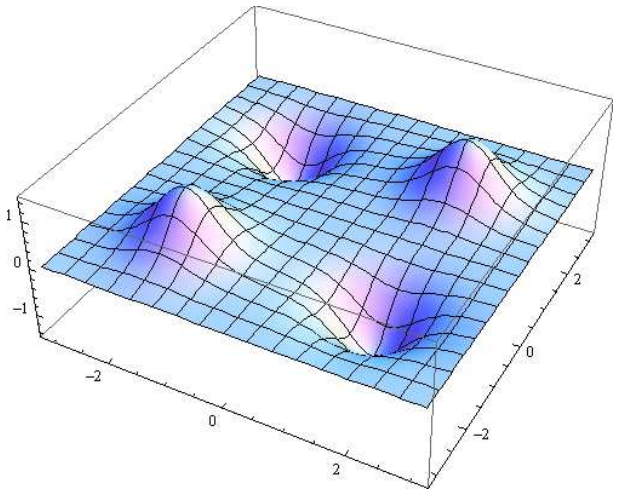


Figure IV.3: The ground state for $\alpha = 0$ and $U = 20$ with a basis of sine functions in both dimensions.

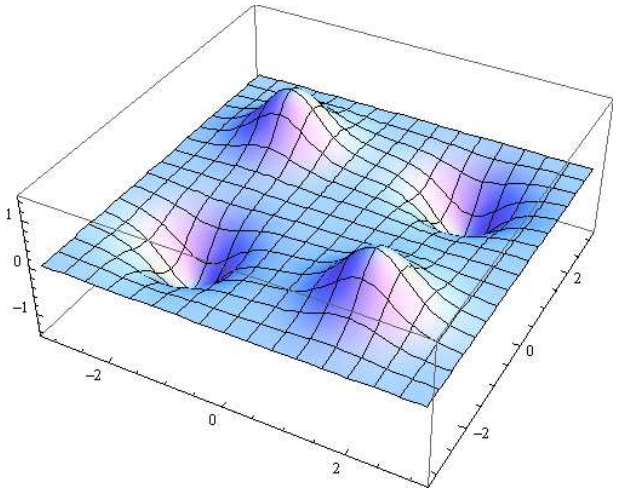


Figure IV.4: The ground state for $\alpha = 0.1$ and $U = 20$ with a basis of sine functions in both dimensions.

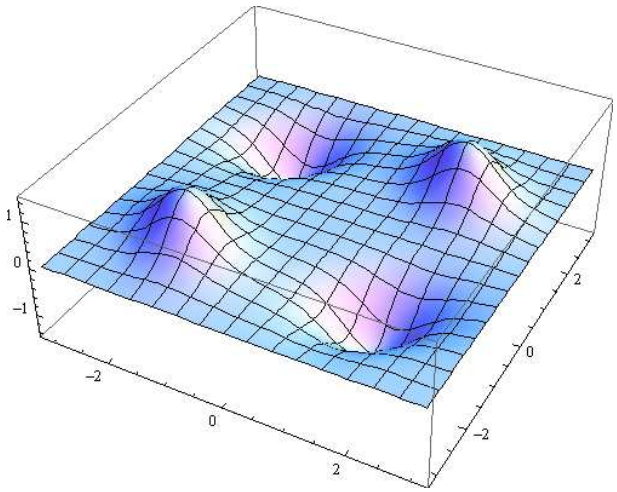


Figure IV.5: The ground state for $\alpha = 0.5$ and $U = 20$ with a basis of sine functions in both dimensions.

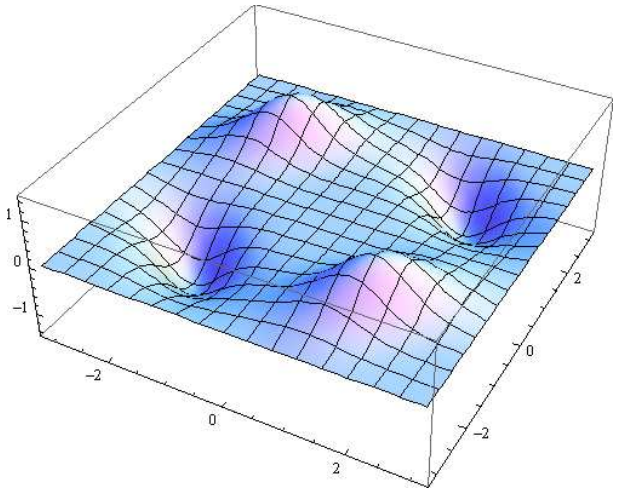


Figure IV.6: The ground state for $\alpha = 0.75$ and $U = 20$ with a basis of sine functions in both dimensions.

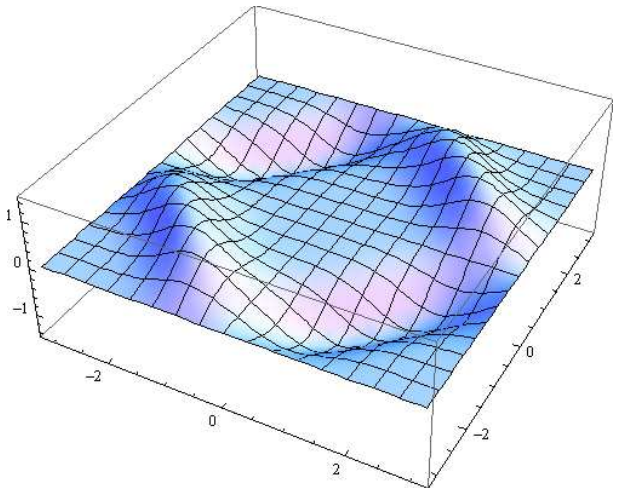


Figure IV.7: The ground state for $\alpha = 1.0$ and $U = 20$ with a basis of sine functions in both dimensions.

# Appendix A

# Action-Angle SoS Code

```
α = 1 / 10
U = 20

j = 1; i = 1; ji = 0; ii = 0;

H = ( (U / kx2) + (U / ky2) +

    α * U * ((Pi^2) / (Sqrt[kx2 * ky2] EllipticK[kx2] * EllipticK[ky2])) *

      Sum_{nx=ii}^{i} Sum_{ny=ji}^{j} Csch[(2 * nx + 1) * (Pi / 2) * (EllipticK[1 - (kx2)] / EllipticK[kx2])] *

        Csch[(2 * ny + 1) * (Pi / 2) * (EllipticK[1 - (ky2)] / EllipticK[ky2])] *

        (Cos[((2 * nx + 1) * θx) - ((2 * ny + 1) * θy)]) ) /.

  {θx -> θx[t], θy -> θy[t], kx2 → kx2[t], ky2 → ky2[t]}

θx11 = {Table[Pi / 2, {n, 1, 10}], Pi, 3 Pi / 2};
θx11 = Flatten[θx11];
kx211 = {Table[0.3 + 0.05 * n, {n, 1, 10}], 0.5, 0.5};
kx211 = Flatten[kx211];
Jx11 = Table[(Sqrt[U / kx211[[n]]] / (Pi)) * (EllipticE[kx211[[n]]]),
   {n, 1, Length[Flatten[θx11]]}];

θx11 = Flatten[θx11];
kx211 = Flatten[kx211];
Jx11 = Flatten[Jx11];

HE = 80;
Table[FindRoot[(H /. {θx[t] → θx11[[n]], θy[t] → 2 Pi, kx2[t] → kx211[[n]]}) == HE,
  {ky2[t], 0.001 * n}], {n, 1, Length[θx11]}]

ky211 = Flatten[N[Re[ky2[t]] /. %], 15] // N

Jy11 =
 Table[(Sqrt[U / ky211[[n]]] / (Pi)) * (EllipticE[ky211[[n]]]), {n, 1, Length[θx11]}]

eq1 = θx'[t] == D[H, kx2[t]] * ( - 2 π U / (EllipticK[kx2[t]] (U / kx2[t])^(3/2)) );

eq2 = Jx'[t] == -D[H, θx[t]];

eq3 = θy'[t] == D[H, ky2[t]] * ( - 2 π U / (EllipticK[ky2[t]] (U / ky2[t])^(3/2)) );

eq4 = Jy'[t] == -D[H, θy[t]];

Jxa = (Sqrt[U / kx2] / (Pi)) * (EllipticE[kx2]);
Jya = (Sqrt[U / ky2] / (Pi)) * (EllipticE[ky2]);
```

```
interpJx =
 Interpolation[{{Jxa /. kx2 -> 0.1 / 20, 0.1 / 20}, {Jxa /. kx2 -> 0.5 / 20, 0.5 / 20},
    {Jxa /. kx2 -> 1 / 20, 1 / 20}, {Jxa /. kx2 -> 1.5 / 20, 1.5 / 20},
    {Jxa /. kx2 -> 2 / 20, 2 / 20}, {Jxa /. kx2 -> 2.5 / 20, 2.5 / 20},
    {Jxa /. kx2 -> 3 / 20, 3 / 20}, {Jxa /. kx2 -> 3.5 / 20, 3.5 / 20},
    {Jxa /. kx2 -> 4 / 20, 4 / 20}, {Jxa /. kx2 -> 4.5 / 20, 4.5 / 20},
    {Jxa /. kx2 -> 5 / 20, 5 / 20}, {Jxa /. kx2 -> 5.5 / 20, 5.5 / 20},
    {Jxa /. kx2 -> 6 / 20, 6 / 20}, {Jxa /. kx2 -> 6.5 / 20, 6.5 / 20},
    {Jxa /. kx2 -> 7 / 20, 7 / 20}, {Jxa /. kx2 -> 7.5 / 20, 7.5 / 20},
    {Jxa /. kx2 -> 8 / 20, 8 / 20}, {Jxa /. kx2 -> 8.5 / 20, 8.5 / 20},
    {Jxa /. kx2 -> 9 / 20, 9 / 20}, {Jxa /. kx2 -> 9.5 / 20, 9.5 / 20},
    {Jxa /. kx2 -> 10 / 20, 10 / 20}, {Jxa /. kx2 -> 10.5 / 20, 10.5 / 20},
    {Jxa /. kx2 -> 11 / 20, 11 / 20}, {Jxa /. kx2 -> 11.5 / 20, 11.5 / 20},
    {Jxa /. kx2 -> 12 / 20, 12 / 20}, {Jxa /. kx2 -> 12.5 / 20, 12.5 / 20},
    {Jxa /. kx2 -> 13 / 20, 13 / 20}, {Jxa /. kx2 -> 13.5 / 20, 13.5 / 20},
    {Jxa /. kx2 -> 14 / 20, 14 / 20}, {Jxa /. kx2 -> 14.5 / 20, 14.5 / 20},
    {Jxa /. kx2 -> 15 / 20, 15 / 20}, {Jxa /. kx2 -> 15.5 / 20, 15.5 / 20},
    {Jxa /. kx2 -> 16 / 20, 16 / 20}, {Jxa /. kx2 -> 16.5 / 20, 16.5 / 20},
    {Jxa /. kx2 -> 17 / 20, 17 / 20}, {Jxa /. kx2 -> 17.5 / 20, 17.5 / 20},
    {Jxa /. kx2 -> 18 / 20, 18 / 20}, {Jxa /. kx2 -> 18.5 / 20, 18.5 / 20},
    {Jxa /. kx2 -> 19 / 20, 19 / 20}, {Jxa /. kx2 -> 19.5 / 20, 19.5 / 20}}, Jx[t]]
interpJy = Interpolation[{{Jya /. ky2 -> 0.5 / 20, 0.5 / 20},
    {Jya /. ky2 -> 1 / 20, 1 / 20}, {Jya /. ky2 -> 1.5 / 20, 1.5 / 20},
    {Jya /. ky2 -> 2 / 20, 2 / 20}, {Jya /. ky2 -> 2.5 / 20, 2.5 / 20},
    {Jya /. ky2 -> 3 / 20, 3 / 20}, {Jya /. ky2 -> 3.5 / 20, 3.5 / 20},
    {Jya /. ky2 -> 4 / 20, 4 / 20}, {Jya /. ky2 -> 4.5 / 20, 4.5 / 20},
    {Jya /. ky2 -> 5 / 20, 5 / 20}, {Jya /. ky2 -> 5.5 / 20, 5.5 / 20},
    {Jya /. ky2 -> 6 / 20, 6 / 20}, {Jya /. ky2 -> 6.5 / 20, 6.5 / 20},
    {Jya /. ky2 -> 7 / 20, 7 / 20}, {Jya /. ky2 -> 7.5 / 20, 7.5 / 20},
    {Jya /. ky2 -> 8 / 20, 8 / 20}, {Jya /. ky2 -> 8.5 / 20, 8.5 / 20},
    {Jya /. ky2 -> 9 / 20, 9 / 20}, {Jya /. ky2 -> 9.5 / 20, 9.5 / 20},
    {Jya /. ky2 -> 10 / 20, 10 / 20}, {Jya /. ky2 -> 10.5 / 20, 10.5 / 20},
    {Jya /. ky2 -> 11 / 20, 11 / 20}, {Jya /. ky2 -> 11.5 / 20, 11.5 / 20},
    {Jya /. ky2 -> 12 / 20, 12 / 20}, {Jya /. ky2 -> 12.5 / 20, 12.5 / 20},
    {Jya /. ky2 -> 13 / 20, 13 / 20}, {Jya /. ky2 -> 13.5 / 20, 13.5 / 20},
    {Jya /. ky2 -> 14 / 20, 14 / 20}, {Jya /. ky2 -> 14.5 / 20, 14.5 / 20},
    {Jya /. ky2 -> 15 / 20, 15 / 20}, {Jya /. ky2 -> 15.5 / 20, 15.5 / 20},
    {Jya /. ky2 -> 16 / 20, 16 / 20}, {Jya /. ky2 -> 16.5 / 20, 16.5 / 20},
    {Jya /. ky2 -> 17 / 20, 17 / 20}, {Jya /. ky2 -> 17.5 / 20, 17.5 / 20},
    {Jya /. ky2 -> 18 / 20, 18 / 20}, {Jya /. ky2 -> 18.5 / 20, 18.5 / 20},
    {Jya /. ky2 -> 19 / 20, 19 / 20}, {Jya /. ky2 -> 19.5 / 20, 19.5 / 20}}, Jy[t]]

eq1 = eq1 /. {kx2[t] → interpJx, ky2[t] → interpJy};
eq2 = eq2 /. {kx2[t] → interpJx, ky2[t] → interpJy};
eq3 = eq3 /. {kx2[t] → interpJx, ky2[t] → interpJy};
eq4 = eq4 /. {kx2[t] → interpJx, ky2[t] → interpJy};
```

```
tmax = 1000;
sol = Table[NDSolve[{eq1, eq2, eq3, eq4, θx[0] == θx11[[n]],
     θy[0] == 2 Pi, Jx[0] == Jx11[[n]], Jy[0] == Jy11[[n]]}, {θx, Jx, θy, Jy},
    {t, 0, tmax}, MaxSteps → 10 000 000, AccuracyGoal → 8], {n, 1, Length[θx11]}]

told = 0; i0 = 1;
tp = Table[Table[If[i > i0, told = tnew];
     θx2 = Mod[θx[t], 4 Pi] /. sol[[n]];
     θy2 = Mod[θy[t], 4 Pi] /. sol[[n]];
     ta = FindRoot[(θy2 == 2 Pi) /. sol[[n]], {t, i}];
     tnew = ta[[1]][[2]];
     If[1 ≤ ta[[1]][[2]] ≤ tmax && tnew ≠ told &&
       Abs[((θy2 - 2 Pi) /. t → ta[[1]][[2]])[[1]]] ≤ 1 * 10^(-8), tnew = ta[[1]][[2]];
      ta[[1]][[2]], -1], {i, i0, tmax, 1}], {n, 1, Length[θx11]}];
tp = Table[Union[tp[[i]]], {i, 1, Length[tp]}];
ThetaJxpts =
  Table[Table[h2 = {Mod[θx[tp[[n]][[i]]], 2 Pi], Jx[tp[[n]][[i]]]} /. sol[[n]],
    {i, 1, Length[tp[[n]]]}], {n, 1, Length[θx11]}];
(*ThetaJxpts=Table[Table[If[ThetaJxpts[[n]][[j]][[1]][[1]]≥Pi,
     ThetaJxpts[[n]][[j]][[1]]=
      {ThetaJxpts[[n]][[j]][[1]][[1]]-2Pi,ThetaJxpts[[n]][[j]][[1]][[2]]},
     {ThetaJxpts[[n]][[j]][[1]][[1]],ThetaJxpts[[n]][[j]][[1]][[2]]}],
    {j,1,Length[tp[[n]]]}],{n,1,Length[θx11]}];*)
ThetaJxpts = Table[Union[ThetaJxpts[[i]]], {i, 1, Length[ThetaJxpts]}];
PSSall =
 Table[ListPlot[ThetaJxpts[[n]], Frame → True, FrameLabel → {"θx", "Jx", None, None},
   PlotStyle → AbsolutePointSize[1], PlotRange → {{-6.3, 6.3}, {-10, 10}},
   DisplayFunction → Identity], {n, 1, Length[ThetaJxpts]}]

ListPlot[ThetaJxpts[[21]], Frame → True,
 FrameLabel → {"θx", "Jx", None, None}, PlotStyle → AbsolutePointSize[1],
 PlotRange → {{-6.3, 6.3}, {-0.1, 2.5}}, DisplayFunction → Identity]

PSSall = Show[PSSall, DisplayFunction → $DisplayFunction,
  PlotRange → {{-0 Pi, 2 Pi}, {-0.1, 5}}, Axes → True, AxesLabel → {"θx", ""}]
```

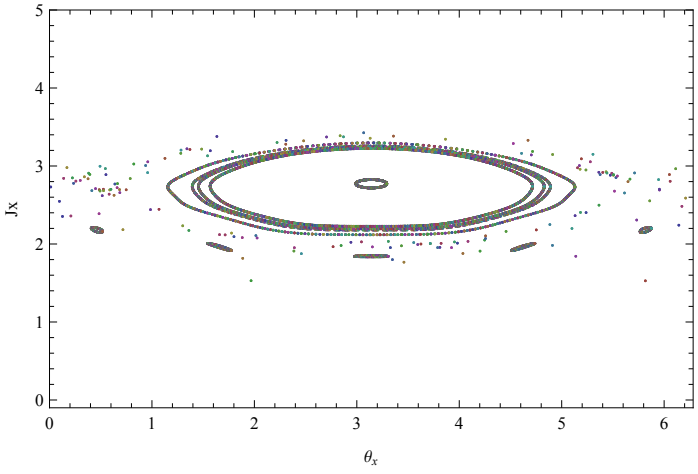

# Appendix B

# Optical Lattice Hamiltonian Eigenstates/Eigenvalues Code

In[10]:=
```
U = 20;
α = 0.1;
```

In[14]:=
```
Integrate[(Sqrt[2 / Pi] * Sin[m * y]) * y * (Sqrt[2 / Pi] * Sin[n * y]), {y, 0, Pi}]
```

Out[14]=
$$\frac{-\frac{1}{(m-n)^2}+\frac{1}{(m+n)^2}+\frac{\cos[(m-n)\pi]}{(m-n)^2}-\frac{\cos[(m+n)\pi]}{(m+n)^2}+\frac{\pi\sin[(m-n)\pi]}{m-n}-\frac{\pi\sin[(m+n)\pi]}{m+n}}{\pi}$$

In[15]:=
```
nmxBETA2 = Table[
  Limit[Limit[(-1/(m-n)^2 + 1/(m+n)^2 + Cos[(m-n) π]/(m-n)^2 - Cos[(m+n) π]/(m+n)^2 + π Sin[(m-n) π]/(m-n) - π Sin[(m+n) π]/(m+n))/π, m → mp], n → np], {mp, 1, 10}, {np, 1, 10}]
```

In[17]:=
```
nmyBETA2 = nmxBETA2
```

In[21]:=
```
EigenvalueX2 = Eigenvalues[N[nmxBETA2]]
```

Out[21]=
```
{2.88443, 2.59226, 2.3002, 2.00836,
 1.71664, 1.42496, 1.13324, 0.84139, 0.549337, 0.257164}
```

In[23]:=
```
EigenvalueY2 = EigenvalueX2
```

Out[23]=
```
{2.88443, 2.59226, 2.3002, 2.00836,
 1.71664, 1.42496, 1.13324, 0.84139, 0.549337, 0.257164}
```

In[24]:=
```
NumEigX2 = Eigenvectors[N[nmxBETA2]]
```

In[25]:=
```
NumEigY2 = NumEigX2

EigenvectorsXdiracbasis2 =
  Table[Sum[NumEigX[[k, n]] * Sqrt[2 / Pi] * Sin[(n) * x], {n, 1, 10}], {k, 1, 10}];

EigenvectorsYdiracbasis2 =
  Table[Sum[NumEigY[[k, n]] * Sqrt[2 / Pi] * Sin[(n) * y], {n, 1, 10}], {k, 1, 10}];
```

In[26]:=
```
Uxeigbasis2 = DiagonalMatrix[Table[(U * Cos[EigenvalueX2[[n]]]^2), {n, 1, 10}]];
Uyeigbasis2 = DiagonalMatrix[Table[(U * Cos[EigenvalueY2[[n]]]^2), {n, 1, 10}]];
Ucoupx2 = DiagonalMatrix[Table[(Cos[EigenvalueX2[[n]]]), {n, 1, 10}]];
Ucoupy2 = DiagonalMatrix[Table[(Cos[EigenvalueY2[[n]]]), {n, 1, 10}]]
```

In[30]:=
```
UxsinebasisWOTP2 = Transpose[NumEigX2].Uxeigbasis2.Inverse[Transpose[NumEigX2]];
UysinebasisWOTP2 = Transpose[NumEigY2].Uyeigbasis2.Inverse[Transpose[NumEigY2]];
UxcouplesineWOTP2 = Transpose[NumEigX2].Ucoupx2.Inverse[Transpose[NumEigX2]];
UycouplesineWOTP2 = Transpose[NumEigY2].Ucoupy2.Inverse[Transpose[NumEigY2]];
```

In[34]:=
```
UCouplingWTP2 = 2 * U * α * KroneckerProduct[UxcouplesineWOTP2, UycouplesineWOTP2]
UxsinebasisWTP2 = KroneckerProduct[UxsinebasisWOTP2, IdentityMatrix[10]];
UysinebasisWTP2 = KroneckerProduct[IdentityMatrix[10], UysinebasisWOTP2];
```

```
KxsinebasisWOTP2 = DiagonalMatrix[Table[(m^2), {m, 1, 10}]];
KysinebasisWOTP2 = DiagonalMatrix[Table[(m^2), {m, 1, 10}]]
```

```
{{1, 0, 0, 0, 0, 0, 0, 0, 0, 0}, {0, 4, 0, 0, 0, 0, 0, 0, 0, 0},
 {0, 0, 9, 0, 0, 0, 0, 0, 0, 0}, {0, 0, 0, 16, 0, 0, 0, 0, 0, 0},
 {0, 0, 0, 0, 25, 0, 0, 0, 0, 0}, {0, 0, 0, 0, 0, 36, 0, 0, 0, 0},
 {0, 0, 0, 0, 0, 0, 49, 0, 0, 0}, {0, 0, 0, 0, 0, 0, 0, 64, 0, 0},
 {0, 0, 0, 0, 0, 0, 0, 0, 81, 0}, {0, 0, 0, 0, 0, 0, 0, 0, 0, 100}}
```

```
KxsinebasisWTP2 = KroneckerProduct[KxsinebasisWOTP2, IdentityMatrix[10]];
KysinebasisWTP2 = KroneckerProduct[IdentityMatrix[10], KysinebasisWOTP2];
```

```
Hsinebasis2 =
 KxsinebasisWTP2 + KysinebasisWTP2 + UxsinebasisWTP2 + UysinebasisWTP2 + UCouplingWTP2
```

```
Eigenvalues[Hsinebasis2]
```

```
Heigenvecsine2 = Eigenvectors[Hsinebasis2]
```

# Bibliography


[1] G. H. Walker and J. Ford, Phys. Rev. **188**, 1 (1969)

[2] E. H. Lieb, Bulletin of the American Mathematical Society **22**, 1 (1990)

[3] E. Wigner, Phys. Rev. **40** (1932) 749

[4] K. Husimi, Proc. Phys. Math. Soc. Jpn. **22** (1940) 264

[5] H. Lee, Physics Reports **259** (1995) 147

[6] A. Hemmerich, D. Schropp, and T. W. Hänsch, Phys. Rev. A **44**, 1910 (1991)

[7] M. Greiner *et al.,* Phys. Rev. Lett. **87**, 160405 (2001)

[8] I. Bloch, Nat. Phys. **1**, 25 (2005)

[9] I. B. Spielman, W. D. Phillips, and J. V. Porto, Phys. Rev. Lett. **98**, 080404 (2007)

[10] D. A. Steck, W. H. Oskay, and M. G. Raizen, Science **293**, 274 (2001)

[11] R. Luter and L. E. Reichl, Phys. Rev. A **66**, 5 (2002)

[12] E. Horsley, S. Koppell, and L. E. Reichl, Phys. Rev. E **89**, 012917 (2014)

[13] R. Grimm, M. Weidemÿller, and Y. B. Ovchinnikov, Adv. At. Mol. Opt. Phys. **42** (2000) 95

[14] B. P. Holder and L. E. Reichl, Phys. Rev. A **76**, 013420 (2007)

[15] F. Gonzalez, G. Drotos, and C. Jung, J. Phys. A: Math. Theor. **47**, 045101 (2014)

[16] P. F. Byrd and M. D. Friedman *Handbook of Elliptic Integrals for Engineers and Physicists* (Springer-Verlag, Berlin, 1954)

[17] D. T. Colbert and W. H. Miller, J. Chem. Phys. **96**, 1982 (1992)

[18] J. C. Light, I. P. Hamilton, and J. V. Lill, J. Chem. Phys. **82**, 1400 (1983)

[19] E. Mathieu, Journal de Mathmatiques Pures et Appliques, 137-203 (1868)

[20] A. J. Laub, *Matrix Analysis for Scientists and Engineers* (Society for Industrial and Applied Mathematics, Philadelphia, 2005)